Macroscopic Vertical Alignment of Nanodomains in Thin Films of Semiconductor Amphiphilic Block Copolymers

Johannes C. Brendel,[†] Feng Liu,[‡] Andreas S. Lang,[†] Thomas P. Russell,[‡] and Mukundan Thelakkat[†,*]

[†]Applied Functional Polymers, Macromolecular Chemistry I, University of Bayreuth, 95440 Bayreuth, Germany and [‡]Polymer Science and Engineering Department, University of Massachusetts, Amherst, Massachusetts 01003, United States

ABSTRACT

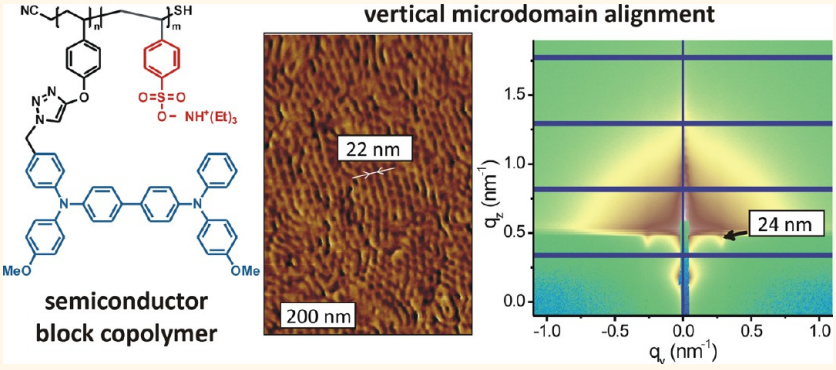

Though several techniques have been reported on the alignment of conventional block copolymers, the macroscopic vertical orientation of semiconductor block copolymer microdomains in thin films has still not been accomplished. Here, we report the control on the alignment of nanostructures in a semiconductor amphiphilic block copolymer comprising an amorphous triphenyldiamine hole conductor block and a hydrophilic poly(styrene sulfonate) segment. Three different compositions with a hole conductor content of 57, 72, and 79 wt % were synthesized using a combination of controlled reversible addition/fragmentation transfer polymerization and "click" chemistry. All polymers feature a narrow molecular weight distribution. Cryo-TEM reveals the formation of micelles in DMF solutions of the amphiphilic copolymer having nanoscopic dimensions. The micelle size correlates well with the X-ray analysis of dried bulk samples. Atomic force microscopy (AFM) confirms the micellar structure in the as-cast films. Thermal annealing causes an aggregation of micelles but did not lead to morphologies known for conventional block copolymers. However, annealing in saturated DMF vapor induces a morphology transition and a vertical orientation of the microdomains which was determined by grazing incidence small-angle X-ray scattering and AFM. The morphology varies from lamella to cylinders with increasing content of the hole-conductor block. The orientation arises from the controlled evaporation of the solvent, a mechanism that is similar to that observed for conventional block copolymers. Our approach demonstrates the macroscopic vertical alignment of nanodomains in semiconductor block copolymers which is a key requirement for applications in hybrid devices.

KEYWORDS: nanostructures · RAFT · click chemistry · controlled polymerization · orientation · solvent annealing · GISAXS

The organization in nanoscopic domains and their alignment are crucial aspects for emerging technologies such as nanomembranes, lithography, microelectronics or organic photovoltaics. Therefore, numerous stategies have been devised to generate periodic patterns on the nanoscale including etching processes or removable templates.[1,2] A promising route toward controlled microdomains is based on the self-organization of block copolymers which self-assemble into well-ordered morphologies ranging from spherical to cylindrical to lamellar domains.[3,4] The size and structure is dictated by the molecular weights and the volume fractions of the individual blocks, respectively. However, most applications require precise control over orientation and alignment of

* Address correspondence to mukundan.thelakkat@uni-bayreuth.de.

Received for review April 16, 2013 and accepted June 7, 2013.

Published online June 07, 2013
10.1021/nn401877g

microdomains.[5,6] While the distinct interaction of the individual blocks with the surface usually favors a parallel alignment, vertical orientation can be achieved by use of an external field. So far electric fields, patterned substrates or controlled solvent interactions have been used to control the spatial orientation of the microdomains.[7−12] The latter has gained increasing attention due to its simplicity, versatility and suitability for many applications.[13−15] The effect of solvents annealing on the alignment of polystyrene−polybutadiene−polystyrene triblock copolymers was first examined by Kim *et al.*[16] Later, detailed work was presented on the orientation of ABC triblock copolymers controlling the evaporation rate of the solvent.[17] Using polystyrene-*b*-poly(ethylene oxide) copolymers, the systematic treatment with benzene vapor leads to well-defined patterns which could be extended to large area macroscopic arrays in combination with structured sapphire substrates.[18,19] And recently, ordered patterns of vertically oriented lamellae with large period distances were obtained combining thermal and solvent annealing.[20] However, up to now no alignment studies on semiconductor block copolymers have been reported except the very recent publication of Goldberg-Oppenheimer *et al.* in which a block copolymer carrying perylene-bisimide pendant groups was aligned using hierarchical electrohydrodynamic lithography.[21]

In this work, we present a block copolymer comprising a semiconductor block and a hydrophilic segment. As hole conductor we use poly(*N*,*N*′-bis(4-methoxyphenyl)-*N*-phenyl-*N*′-4-triazolylphenyl-(1,1′-biphenyl)-4,4′-diamine (PDMTPD). The tetraphenylbenzidine group is well-known for its highly reversible oxidation and hole transport properties. Charge carrier mobilities of 1×10^{-3} $cm^2/(V\ s)$ have been observed in side-chain functionalized polymers.[22] Another important point for selecting PDMTPD building block for this work is the amorphous nature of the PDMTPD block so that solvent vapor treatment earlier reported for conventional coil−coil block copolymers can be adapted here.[23]

Poly(triethylammonium styrene sulfonate) (PEt_3NH^+SS) features some unique properties as hydrophilic block due to the strong ionic sulfonate group. These groups are permanently charged down to a pH of 1 turning them into ideal counterparts for metal salt precursors or electrostatically stabilized inorganic nanoparticles which do not necessitate any insulating ligands for solubilization.[24−26] Furthermore, the sulfonate groups are known to catalyze the hydrolysis of TiO_2 precursors to the anatase structure at low temperatures of 40 °C which is otherwise usually observed at temperatures above 400 °C.[27,28]

The bulk morphology of the prepared semiconductor amphiphilic block copolymer before and after thermal annealing was analyzed with small-angle X-ray scattering (SAXS). Solution structures in DMF were examined using cryo transmission electron microscopy (TEM). Furthermore, thin films were prepared and characterized. The orientation and morphology of as-cast, thermal annealed and solvent treated thin films were analyzed with atomic force microscopy (AFM) and grazing incidence small-angle X-ray scattering (GISAXS).

RESULTS AND DISCUSSION

Synthesis. Among the controlled polymerization techniques, the reversible addition−fragmentation chain transfer (RAFT) process is a versatile tool for preparation of functional polymers.[29−31] The required chain transfer agents (CTA) are already commercially available and optimized for various types of monomers. Nevertheless, the controlled polymerization of bulky and reactive monomers, as they are used for electronic applications, remains challenging.[32,33] Recently, we presented a combined approach using controlled radical polymerizations and copper-catalyzed azide−alkyne cycloaddition (CuAAC, "click" chemistry) to prepare well-defined polymers carrying perylene bisimide groups.[34] The advantage of well-defined scaffold polymers from controlled polymerization techniques along with the flexibility and high yields of "click"-reactions makes it a versatile route toward tailor-made functional polymers.

Accordingly, we prepared the desired block copolymer PDMTPD-*b*-PEt_3NH^+SS **8** in a multistep synthesis, presented in Scheme 1. First the precursor polymer poly(4-(3-trimethylsilylpropargyloxy)styrene)-*block*-poly(2,2,2-trifluorethyl styrene sulfonate) (PTMSPS-*b*-PTfeSS **4**) was polymerized *via* stepwise RAFT polymerization using *S*-cyanomethyl-*S*-dodecyltrithiocarbonate as CTA. The monomer 4-(3-trimethylsilylpropargyloxy)-styrene (TMSPS **1**) was prepared according to literature procedures.[34] After deprotection of the alkyne group, the hole conductor moiety was attached by CuAAC of the azide *N*,*N*′-bis(4-methoxyphenyl)-*N*-phenyl-*N*′-4-azidophenyl-(1,1′-biphenyl)-4,4′-diamine dimethoxy triphenyl diamine (DMTPD-N_3 **6**). The detailed synthesis procedure for DMTPD-N_3 is given in the Supporting Information (Figure S1). The resulting poly(*N*,*N*′-bis-(4-methoxyphenyl)-*N*-phenyl-*N*′-4-triazolylphenyl-(1,1′-biphenyl)-4,4′-diamine)-*block*- poly(2,2,2-trifluorethyl styrene sulfonate) (PDMTPD-*b*-PTfeSS **7**) was converted to poly(*N*,*N*′-bis(4-methoxyphenyl)-*N*-phenyl-*N*′-4-triazolyl-phenyl-(1,1′-biphenyl)-4,4′-diamine)-*block*-poly(triethyl-ammonium styrene sulfonate) *via* basic hydrolysis of the sulfonate ester.

Characterization. The individual intermediates were characterized by NMR and SEC measurements to ensure that no side reactions occur and a well-defined polymer was formed. The SEC traces of selected steps are shown in Figure 1a.

In all cases, a narrow distribution was retained. Only for the large molecular weight polymers (PDMTPD-*b*-PTfeSS **7c**) some interchain coupling was detected, which can be related to disulfide coupling after partial

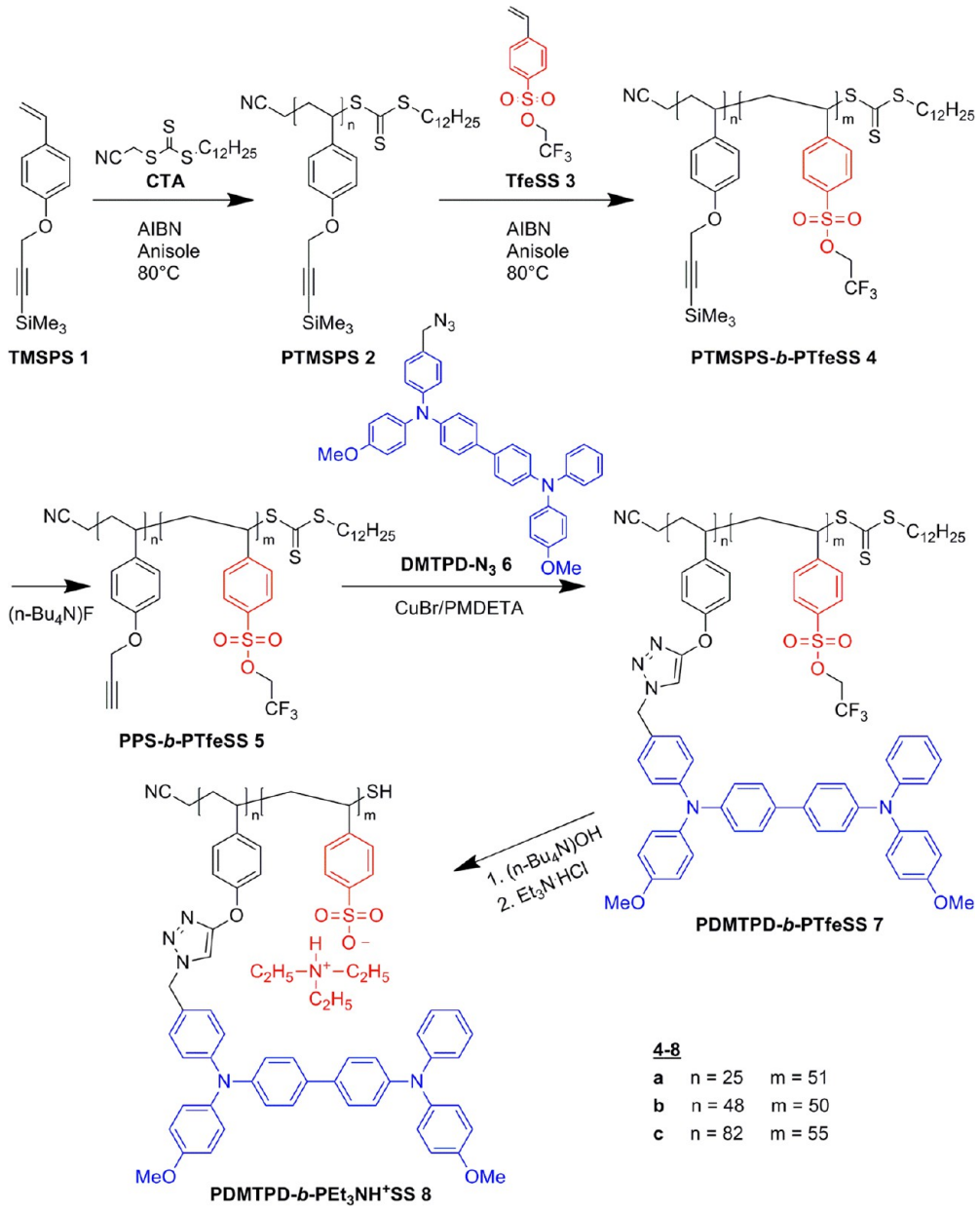

Scheme 1. Synthesis procedure for poly(*N*,*N*′-bis(4-methoxyphenyl)-*N*-phenyl-*N*′-4-triazolylphenyl-(1,1′-biphenyl)-4,4′-diamine)-*block*- poly(triethylammonium styrene sulfonate). (AIBN, 2,2′-Azobis(2-methylpropionitrile); PMDETA, *N*,*N*,*N*′,*N*′,*N*″-pentamethyldiethylenetriamine)

loss of the CTA end-group or alkyne−alkyne coupling reactions. Nevertheless, the diblock copolymer formation and all polymer analogous reaction steps can be assumed to be quantitative, since no residual peaks of macro-CTA or precursor polymers were observed in SEC (Figure 1a). As no residual alkyne protons were traceable in NMR analysis, we conclude >95% (considering the error limit of NMR) "click" efficiency for the CuAAC. The number average molecular weights M_n, the polydispersity indices (PDI) and the average molecular weights calculated from the NMR spectra are summarized in Table 1.

Accordingly, we prepared three different block copolymers varying the composition of the individual blocks. The block copolymers **8a**, **8b**, and **8c** contain 57, 72, and 79 wt % of PDMTPD, respectively. The characteristics of the final polymers PDMTPD-*b*-PEt$_3$NH$^+$SS **8a**−**c** and the respective precursors PDMTPD-*b*-PTfeSS **7a**−**c** are also included in Table 1, whereas the SEC traces of the precursors are shown in Figure 1b. Details on the SEC analysis of all intermediate steps for the different block copolymers are given in the Supporting Information (Figure S2). To prove a unimodal growth of the second block the samples were additionally monitored in SEC with different eluent (THF with 0.25% tetrabutylammonium bromide salt which was added to reduce the interaction of the polymer with the column) (Figure S3). All polymers exhibit narrow molecular

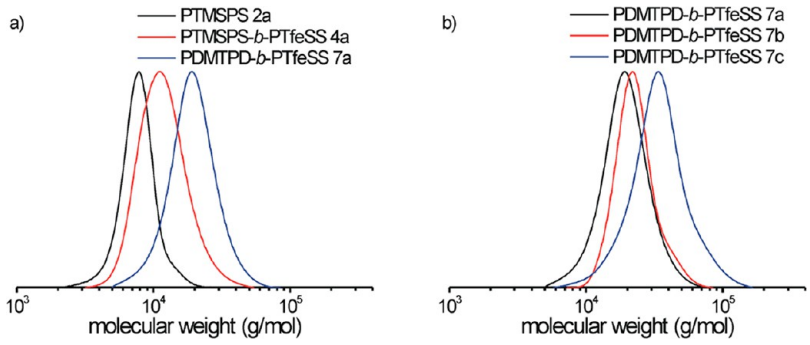

Figure 1. (a) Normalized SEC traces of the intermediate steps poly(4-(3-trimethylsilylpropargyloxy)styrene) (PTMSPS 2a, black), poly(4-(3-trimethylsilylpropargyloxy)styrene)-*block*-poly(2,2,2-trifluorethyl styrene sulfonate) (PTMSPS-*b*-PTfeSS 4a, red) and poly(*N*,*N*′-bis(4-methoxyphenyl)-*N*-phenyl-*N*′-4-triazolylphenyl-(1,1′-biphenyl)-4,4′-diamine)-*block*- poly(2,2,2-trifluorethyl styrene sulfonate) (PDMTPD-*b*-PTfeSS 7a, blue). (b) Normalized SEC traces of the different block copolymer precursors PDMTPD-*b*-PTfeSS 7a, PDMTPD-*b*-PTfeSS 7b and PDMTPD-*b*-PTfeSS 7c. The final polymers PDMTPD-*b*-PEt$_3$NH$^+$SS could not be measured in SEC due to a strong interaction of the polyelectrolyte with the column material. The SEC was calibrated according to polystyrene standards.

TABLE 1. M_n and PDI Measured by SEC and an Average Molecular Weight Calculated from the NMR Spectra for the Intermediate Steps in the Synthesis of PDMTPD-*b*-PEt$_3$NH$^+$SS 8a, for All Nonionic Precursors PDMTPD-*b*-PTfeSS 7a–c and the Respective Final Polymers PDMTPD-*b*-PEt$_3$NH$^+$SS 8a–c

sample	M_n (SEC)[a]	PDI (SEC)[a]	MW (NMR)[a]	wt % PDMTPD
PTMSPS **2a**	7.3 kg/mol	1.09	6.1 kg/mol	-
PTMSPS-*b*-PTfeSS **4a**	10.7 kg/mol	1.17	19.5 kg/mol	-
PDMTPD-*b*-PTfeSS **7a**	17.6 kg/mol	1.17	33.0 kg/mol	58 wt %
PDMTPD-*b*-PTfeSS **7b**	21.6 kg/mol	1.12	50.0 kg/mol	72 wt %
PDMTPD-*b*-PTfeSS **7c**	30.1 kg/mol	1.26	77.6 kg/mol	81 wt %
PDMTPD-*b*-PEt$_3$NH$^+$SS **8a**[c]	-	-	34.0 kg/mol	57 wt %
PDMTPD-*b*-PEt$_3$NH$^+$SS **8b**[c]	-	-	51.0 kg/mol	72 wt %
PDMTPD-*b*-PEt$_3$NH$^+$SS **8c**[c]	-	-	79.0 kg/mol	79 wt %

[a] The SEC was calibrated according to polystyrene standards. [n] For calculation of the PTMSPS block, the ratio of the signals at 4.63 ppm and 3.22 ppm of the polymer and the RAFT end-group, respectively, were taken. The MW of the PTfeSS block was calculated from the ratio of the two blocks, *viz.*, the signals at 4.82 ppm (PTfeSS) and 4.67 ppm (PTMSPS). [c] The final polymer PDMTPD-*b*-PEt$_3$NH$^+$SS could not be measured by SEC due to strong interactions with the column material.

weight distributions. Assuming densities of 1–1.2 g/mL, which is common for amorphous polymers, sample PDMTPD-*b*-PEt$_3$NH$^+$SS **8a** possesses a volume ratio suitable for a lamellar morphology. On the other hand, PDMTPD-*b*-PEt$_3$NH$^+$SS **8b** should lead to cylindrical domains and PDMTPD-*b*-PEt$_3$NH$^+$SS **8c** may even form a spherical morphology in thin films.

The thermal characterization of the polymers reveals a decomposition onset of 300–310 °C independent of the composition. In the differential scanning calorimetry (DSC) the individual block copolymers show only one T_g, which shifts to higher values for increasing number of PDMTPD repeating units (Figure S4). For PDMTPD-*b*-PEt$_3$NH$^+$SS **8a**, we found a T_g of 144 °C, for PDMTPD-*b*-PEt$_3$NH$^+$SS **8b** 162 °C and for PDMTPD-*b*-PEt$_3$NH$^+$SS **8c** 178 °C. No difference was found for the precursor polymers PDMTPD-*b*-PTfeSS **7a**–**c**. The T_g values are in the same range as those reported for DMTPD pendant homopolymers.[22]

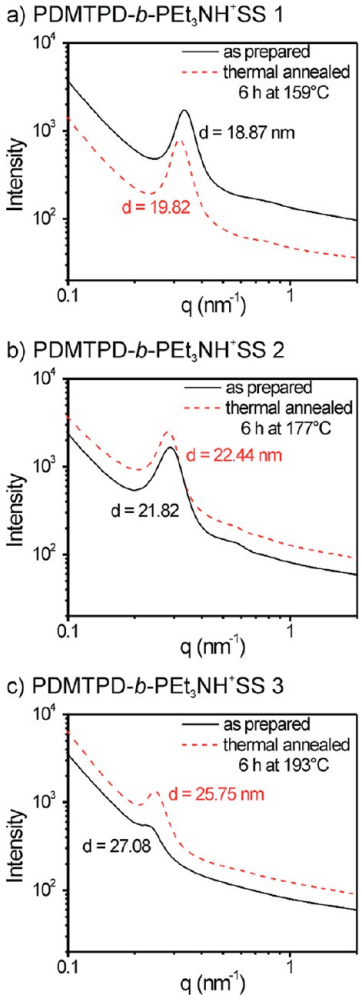

Figure 2. Small angle X-ray spectroscopy (SAXS) results on bulk samples of the different block copolymers (a) PDMTPD-*b*-PEt$_3$NH$^+$SS 8a, (b) PDMTPD-*b*-PEt$_3$NH$^+$SS 8b and (c) PDMTPD-*b*-PEt$_3$NH$^+$SS 8c; black solid line, before annealing over T_g; red dashed line, after annealing over T_g for 6 h. The distances *d* are calculated from the respective peak maxima.

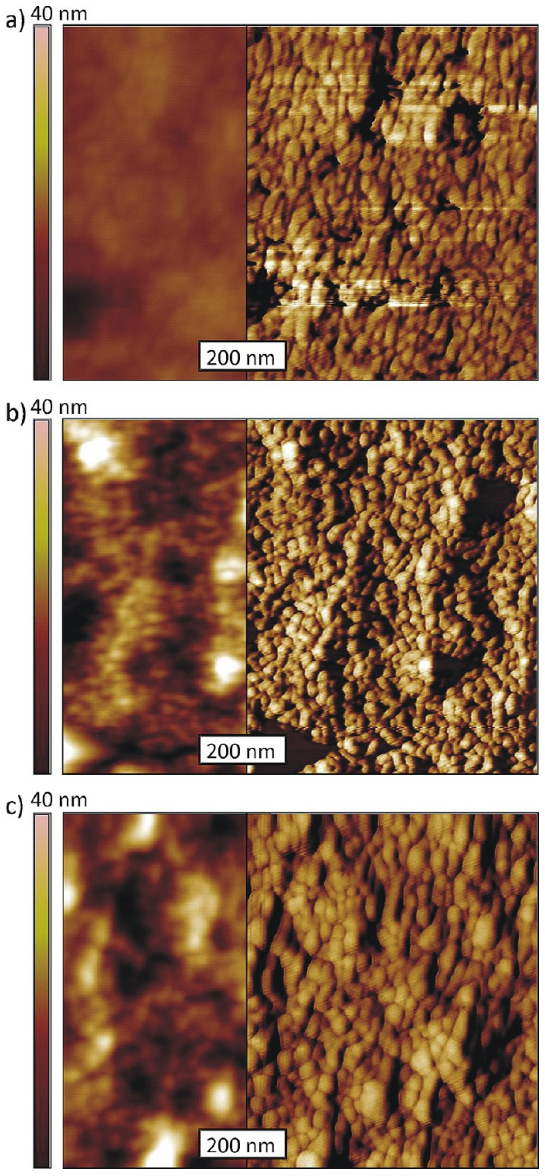

Figure 3. AFM height (left) and phase (right) images of thin films made by spin-casting a 10 wt % solution of PDMTPD-*b*-PEt_3NH^+SS 8a (a), PDMTPD-*b*-PEt_3NH^+SS 8b (b) and PDMTPD-*b*-PEt_3NH^+SS 8c (c) in DMF.

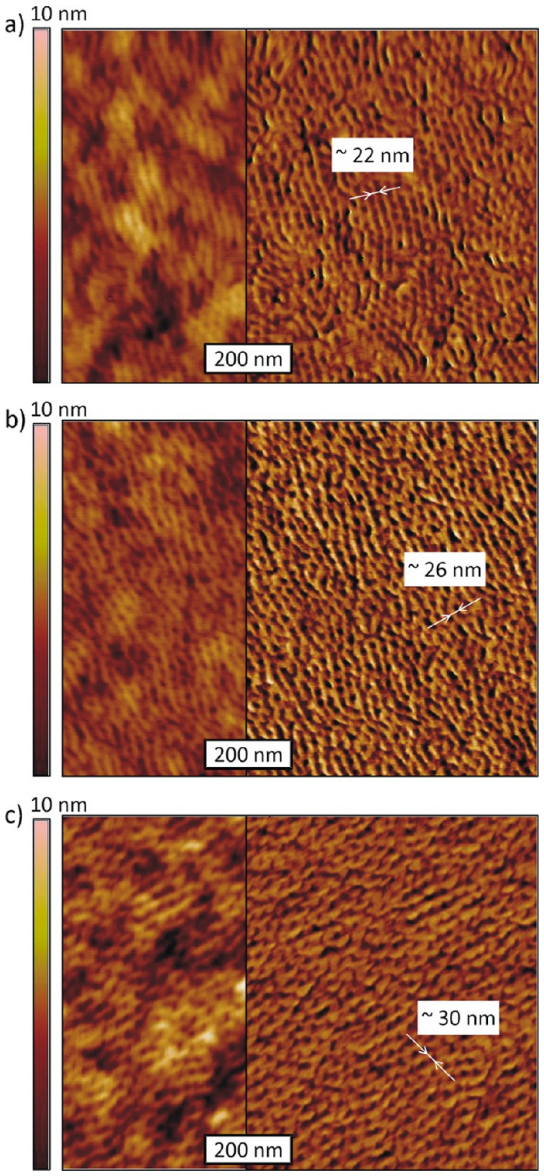

Figure 4. AFM height (left) and phase (right) images of thin films made by spin-casting a 10 wt % solution of PDMTPD-*b*-PEt_3NH^+SS 8a (a), PDMTPD-*b*-PEt_3NH^+SS 8b (b) and PDMTPD-*b*-PEt_3NH^+SS 8c (c) in DMF. The films were annealed in saturated DMF vapor for 4 days.

Two-dimensional small-angle X-ray scattering (SAXS) of bulk samples was performed at the National Synchrotron Light Source (NSLS) at the Brookhaven National Laboratory (BNL). One-dimensional SAXS profiles were obtained by circular averaging of the corresponding two-dimensional scattering patterns. The results are shown in Figure 2. As we can see, all these samples show a certain length scale of phase separation defined by the major peak in the scattering profiles. For sample PDMTPD-*b*-PEt_3NH^+SS **8a**, a center-to-center distance of 18.9 nm was calculated from the major peak. Increasing the PDMTPA content to 72% (**8b**), the feature size of the phase separation is increased to 21.8 nm. Further increase of PTMTPA content (**8c**) elevates the phase separation size to 25.7 nm. It has to be noted we can only see first order correlation in the scattering profiles. No microdomain nanostructures, as observed in conventional AB-diblock copolymers such as cylinders or lamellae, are found. Thermal annealing slightly increases the center-to-center distances for all three samples with data labeled in Figure 2. Although the PDMTPD-block becomes flexible, the strong interactions of the sulfonate groups in PEt_3NH^+SS may prevent the movement of the polymer chains.

Analysis of Thin Films. The block copolymers PDMTPD-*b*-PEt_3NH^+SS **8a**–**c** were deposited on a silicon substrate covered with a thin layer of ZnO by spin-casting a 10 wt % solution of the polymers in DMF resulting in a layer of approximately 150 nm. The morphology was examined by AFM and GISAXS.[35,36] The untreated

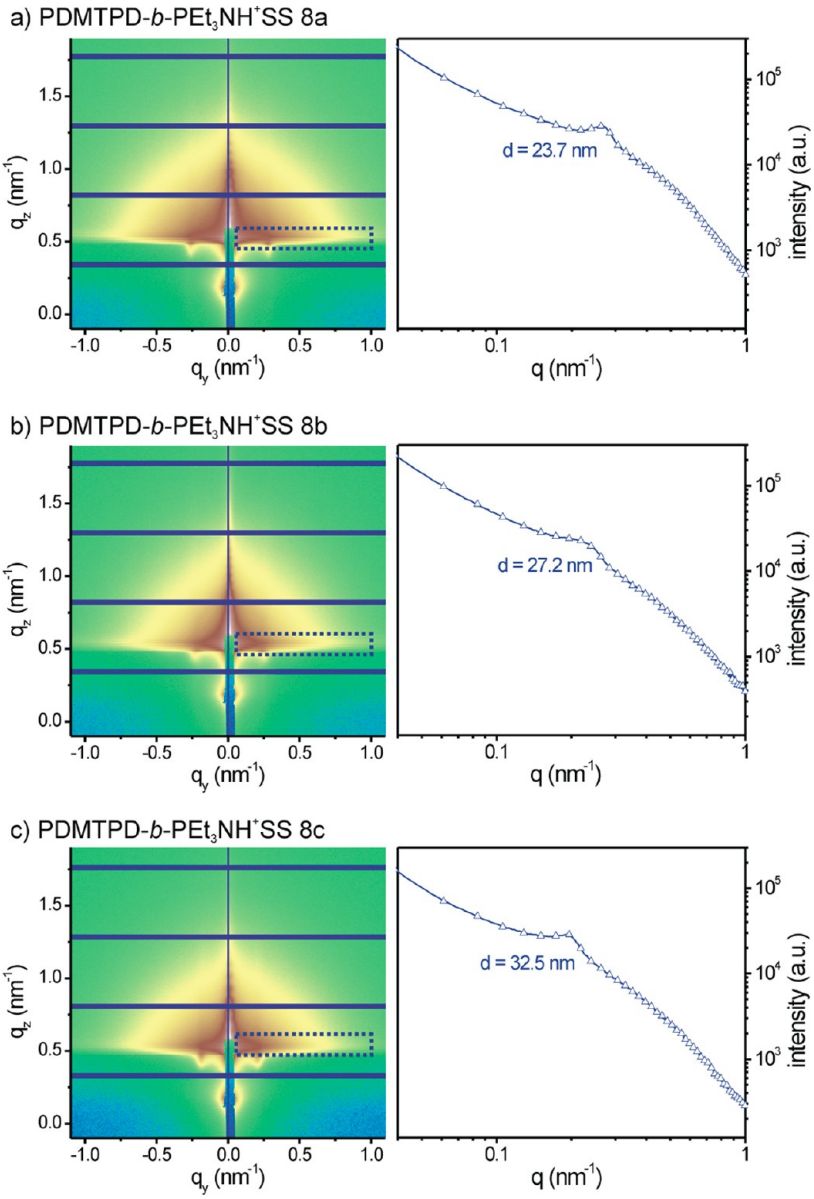

Figure 5. GISAXS measurements of the solvent annealed thin films made of PDMTPD-*b*-PEt$_3$NH$^+$SS 8a (a), PDMTPD-*b*-PEt$_3$NH$^+$SS 8b (b) and PDMTPD-*b*-PEt$_3$NH$^+$SS 8c (c); the plots on the right show the indicated in-plane line cuts (dotted rectangle) out of the full pattern (left). For each signal, the calculated *d*-spacing is assigned.

films of PDMTPD-*b*-PEt$_3$NH$^+$SS show no repetitive pattern, but spherical structures for all the samples as observed in AFM which arise from the formation of micelles (Figure 3). Further evidence for micelle formation could be observed exemplarily in cryo-TEM images of a solution of the polymer PDMTPD-*b*-PEt$_3$NH$^+$SS **8c** in DMF (Figure S5). The average size of the micelles in the images was estimated to be 27 nm which is in very good agreement with the SAXS signal of the bulk samples (d = 27.08 nm before annealing) and the structure sizes found in the AFM micrographs (average size 28 nm) for the sample PDMTPD-*b*-PEt$_3$NH$^+$SS **8c**. This effect further explains the high roughness of the films which is caused by the aggregation of the micelles during the drying process.

The size of the spherical structures grows with increasing content of PDMTPD from 22 nm (**8a**) to 24 nm (**8b)** and finally to 28 nm on block copolymer **8c**. During the casting process, the soft micelles are flattened and, in consequence, the sizes are slightly larger than the average distance found in the SAXS analysis of the dried bulk samples (19, 22, and 27 nm). Nevertheless, the increase in structure size from block copolymer **8a** to **8b** and **8c** is comparable in both AFM and SAXS. GISAXS analysis of all thin films gave no evidence for order in the morphology of those films (Figure S6).

To promote the self-assembly, the films were annealed either by thermal treatment above T_g or by continuous exposure to saturated solvent vapor. Analogous to the

bulk samples, thermal annealing did not significantly alter the structure in the thin films. Only the PDMTPD phase was able to rearrange slightly leading to an increased aggregation of the micelles during the annealing. The GISAXS measurements and AFM images are given in the Supporting Information (Figure S7 and Figure S8). Alternatively, the effects of continuous solvent annealing in DMF vapor were examined. DMF is an excellent solvent for PEt_3NH^+SS, while it is only a moderate solvent for PDMTPD. The preferential interaction of DMF with the PEt_3NH^+SS block should lead to a strong swelling of its domain, while the PDMTPD domains take up less solvent. For solvent annealing the samples were kept in sealed chambers with a solvent reservoir and were analyzed after 4 days of annealing. We chose this long time period to enable the reorganization of the polymer chains in accordance with experience in previous experiments. Since the sterically demanding DMTPD side groups restrict the chain movement a long time scale was chosen. The AFM images of the resulting thin films are depicted in Figure 4.

The surface patterns in the AFM images clearly reveal a reorganization of the block copolymer toward more ordered domains in contrast to the as-spun films (Figure 4). The microdomains feature lamellar morphology in polymer **8a** and cylinder morphology in sample **8c** with domain sizes changing from 21 to 30 nm. Images with lower magnification give evidence for a uniform large scale effect of the solvent vapor treatment (Figure S9). Furthermore, discrete peaks emerge in the in-plane GISAXS pattern which confirm a morphology oriented perpendicular to the substrate (Figure 5).

No out of plane signals arise corroborating an exclusively vertical orientation of the block copolymer domains in the film. In conjunction with the AFM images, a vertical lamellar structure can be attributed for the sample PDMTPD-*b*-PEt_3NH^+SS **8a** indicated by the meander like structures on the surface. However, these forms are regularly interrupted. Keeping the weight ratio of PDMTPD/PEt_3NH^+SS of 58/42 in mind, a lamellar morphology is expected, but the strong dipole interactions of the sulfonate groups may interfere with a full morphology transition from micelles in the as-cast state to a lamellar morphology after annealing. In sample PDMTPD-*b*-PEt_3NH^+SS **8b** (PDMTPD/PEt_3NH^+SS of 72/28), the cylindrical structure becomes more pronounced, although some areas still show short lamellae sections. The sample PDMTPD-*b*-PEt_3NH^+SS **8c**, with a ratio of 79/21, clearly depicts a dot-like surface representative for vertical aligned cylinders. In contrast to the expected equilibrium morphologies which are commonly observed by thermal annealing of conventional diblock copolymers, solvent treatment may alter the volume ratios due to a preferential interaction with one block. Similar observations were found for polystyrene-*block*-poly(vinyl pyridine) copolymers treated with various compositions of toluene and THF vapor which clearly influence the resulting morphology transition from micelles to cylindrical microdomains.[37] Here, we observe a similar transition with the selective solvent DMF but in film thicknesses exceeding the period size of the polymer (Figure 6). In consequence, we assume a solvent evaporation effect causing the vertical alignment of the block copolymer similar as that observed for PS-*b*-PEO copolymers.[18] In this case, a gradient of solvent in the thin film induces the orientation propagating through the film during solvent evaporation.

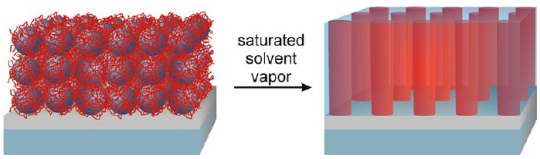

Figure 6. Schematic representation of the morphology transition from nonordered micelles toward vertically aligned cylindrical microdomains upon treatment with saturated solvent vapor.

CONCLUSIONS

In conclusion, we demonstrated the alignment of a functional amphiphilic block copolymer comprising the semiconducting segment PDMTPA and a hydrophilic polyanion block PEt_3NH^+SS in vertical oriented microdomains upon solvent annealing. A key requirement for this control on morphology is first of all the preparation of well-defined block copolymers which is still a challenge for bulky functional groups. Therefore, we established a synthesis procedure combining the advantages of RAFT polymerization with the "click" chemistry approach to obtain narrowly distributed block copolymers with defined segment lengths. Utilizing this synthesis technique, we prepared three different compositions of variable PDMTPD content. The copolymers form micelles in DMF solutions which were retained in the as-cast thin films. Thermal treatment of the polymers did not notably affect the morphology either in the bulk or in the thin film. This can be attributed to the strong interactions of the ionic sulfonate groups suppressing the reorientation of the polymer chains. However, treating the thin films with saturated vapor of DMF induces a morphology transition. Thus, a lamellar morphology was obtained for the copolymer with low PDMTPD content. Increasing the content alters the structure toward cylindrical microdomains oriented perpendicular to the substrate which was supported by AFM and GISAXS measurements. While this perpendicular orientation was so far only reported for conventional block copolymers, we, for the first time, demonstrated the controlled vertical alignment of a semiconductor block copolymer. This promising development is suitable for a wide range

of applications in hybrid systems, since the hydrophilic block enables the incorporation of inorganic materials.[38,39] Furthermore, due to the versatility of the combination of RAFT and "click" chemistry, this modular synthetic procedure can conveniently be extended to a large variety of functional groups.

EXPERIMENTAL SECTION

Materials and Methods. The synthesis of poly(propargyl oxystyrene) was shown elsewhere.[1] The chain transfer agent (CTA) *S*-cyanomethyl-*S*-dodecyltrithiocarbonate (97%) was purchased from ABCR Germany. Dimethylformamide (99.8%) was purchased from Sigma-Aldrich. PMDETA (≥98%) was purchased from Fluka. CuBr (98%) was bought from Acros. All reagents were used without further purification unless otherwise noted. ^{1}H NMR (300 MHz) spectra were recorded on a Bruker AC 300 spectrometer and calibrated according to the respective solvent resonance signal. SEC measurements were carried out either in pure THF or in THF with 0.25% tetrabutylammonium-bromide with two Varian MIXED-C columns (300 × 7.5 mm) at room temperature and at a flow rate of 0.5 mL/min using UV (Waters model 486) with 254 nm detector wavelength and refractive index (Waters model 410) detectors. Polystyrene in combination with *o*-DCB as an internal standard was used for calibration. Differential scanning calorimetry experiments were conducted at heating rates of 10 K·min^{-1} under N_2 atmosphere with a Perkin-Elmer Diamond DSC calibrated with indium. Thermogravimetry measurements were conducted on a Mettler Toledo TGA/SDTA 851^e under N_2 atmosphere at a heating rate of 10 K/min. Temperature of decomposition (T_{onset}) was calculated from the onset of the respective curve. Atomic force microscopy was conducted on a Dimension 3100 Nanoscope IV instrument with a closed-loop XY tip-scanner in the tapping mode. Thermal annealing was conducted under N_2 above the estimated T_g. For solvent annealing, the samples were kept in a closed vessel with a respective solvent reservoir.

Two-dimensional small-angle X-ray scattering (SAXS) was performed at the beamline X27C, National Synchrotron Light Source (NSLS), Brookhaven National Laboratory (BNL). The wavelength of incident X-ray was 0.1371 nm. Scattering signals were collected by a marCCD 2D detector with a resolution of 79 mm/pixel. Typical exposure time was between 30 and 120 s. All the SAXS data presented here are raw data without background subtraction. One-dimensional SAXS profiles were obtained by circular averaging of the corresponding two-dimensional scattering patterns. Grazing incidence small-angle X-ray scattering (GISAXS) was carried out at beamline 7.3.3 Advanced Light Source (ALS), Lawrence Berkeley National Lab (LBNL). An X-ray beam was impinged onto the sample at 0.2° grazing angle slightly above the critical angle of the polymer film (R_c = 0.16°) but below the critical angle of Si substrates (R_c = 0.28°). The wavelength of X-rays used was 1.240 Å, and the scattered intensity was detected by using a Pilatus 1 M detector with image sizes of 981 × 1043 pixels.

Synthesis Procedures for the Preparation of the Block Copolymers. A detailed synthesis procedure is representatively given for the sample PDMTPD-*b*-PEt$_3$NH$^+$SS **8a**. The conditions were kept constant for all samples, but the amounts of reagents were adjusted to obtain the desired molecular weights.

Poly(4-(3-trimethylsilylpropargyloxy)styrene) (PTMSPS 2a). Under nitrogen, 4-(3-trimethylsilylpropargyloxy)styrene (3 g, 13.3 mmol), *S*-cyanomethyl-*S*-dodecyltrithiocarbonate (0.085 g, 0.27 mmol) and 2,2′-azobisisobutyronitrile (8.8 mg, 0.05 mmol) were dissolved in 3 mL of anisole. The reaction mixture was degassed by 5 freeze−thaw cycles and the reaction was started in an oil bath at 80 °C. After 4.5 h, the reaction was stopped at a conversion of approximately 50% by immersing the flask into an ice bath. For purification, the polymer was diluted with chloroform and precipitated in methanol twice. Filtration gave 1.3 g (80%) of yellowish powder of poly(4-(3-trimethylsilylpropargyloxy)styrene). ^{1}H NMR (300 MHz, $CHCl_3$): δ (ppm) 6.9−6.18 (br m, 100H, Ar*H*), 4.63 (s, 50H, −O*CH*$_2$), 3.22 (t, 2H, −S−*CH*$_2$−C$_{11}$H$_{23}$), 2.10−0.92 (br m, 97H, backbone *CH*, *CH*$_2$, CN−*CH*$_2$−S−, −S−*CH*$_2$−C$_{10}$*H*$_{20}$−CH$_3$), 0.90 (t, 3H, -C$_{11}$H$_{22}$−*CH*$_3$), 0.23 (m, 225H, Si*Me*$_3$). SEC: M_n = 7300 g mol^{-1}; PDI = 1.09.

PTMSPS 2b. 4-(3-Trimethylsilylpropargyloxy)styrene (2.7 g, 11.6 mmol), *S*-cyanomethyl-*S*-dodecyltrithiocarbonate (0.037 g, 0.12 mmol), 2,2′-azobisisobutyronitrile (3.8 mg, 0.02 mmol). ^{1}H NMR (300 MHz, $CHCl_3$): δ (ppm) 6.9−6.18 (br m, 192H, Ar*H*), 4.63 (s, 96H, −O*CH*$_2$), 3.22 (t, 2H, −S−*CH*$_2$−C$_{11}$H$_{23}$), 2.10−0.92 (br m, 166H, backbone *CH*, *CH*$_2$, CN−*CH*$_2$−S−, −S−*CH*$_2$−C$_{10}$*H*$_{20}$−CH$_3$), 0.90 (t, 3H, −C$_{11}$H$_{22}$−*CH*$_3$), 0.23 (m, 432H, Si*Me*$_3$). SEC: M_n = 11 500 g mol^{-1}; PDI = 1.11.

PTMSPS 2c. 4-(3-Trimethylsilylpropargyloxy)styrene (2.7 g, 11.6 mmol), *S*-cyanomethyl-*S*-dodecyltrithiocarbonate (0.037 g, 0.12 mmol), 2,2′-azobisisobutyronitrile (3.8 mg, 0.02 mmol). ^{1}H NMR (300 MHz, $CHCl_3$): δ (ppm) 6.9−6.18 (br m, 328H, Ar*H*), 4.63 (s, 164H, −O*CH*$_2$), 3.22 (t, 2H, −S−*CH*$_2$−C$_{11}$H$_{23}$), 2.10−0.92 (br m, 268H, backbone *CH*, *CH*$_2$, CN−*CH*$_2$−S−, −S−*CH*$_2$−C$_{10}$*H*$_{20}$−CH$_3$), 0.90 (t, 3H, -C$_{11}$H$_{22}$−*CH*$_3$), 0.23 (m, 738H, Si*Me*$_3$). SEC: M_n = 11 500 g mol^{-1}; PDI = 1.11.

Poly(4-(3-trimethylsilylpropargyloxy)styrene)-*block*-poly(2,2,2-trifluorethyl styrene sulfonate) (PTMSPS-*b*-PTfeSS 4a). Under nitrogen, PTMSPS **2a** (0.5 g, 0.08 mmol), 2,2,2-trifluoroethyl 4-vinylbenzenesulfonate (2.2 g, 8.2 mmol) and 2,2′-azobisisobutyronitrile (4.1 mg, 0.025 mmol) were dissolved in 1.2 mL of 2-butnaone. The reaction mixture was degassed by 5 freeze−thaw cycles and the reaction was started in an oil bath at 80 °C. After 140 min, the reaction was stopped by immersing the flask into an ice bath. For purification, the polymer was diluted with THF and precipitated in methanol twice. Filtration gave 1.1 g (66%) of yellowish powder of poly(4-(3-trimethylsilylpropargyloxy)styrene)-*block*-poly(2,2,2-trifluorethyl styrene sulfonate). ^{1}H NMR (300 MHz, DMSO-d_6): δ (ppm) 7.83−7.50 (m, 102H, aromatic −*CH*═C−SO$_3$−), 7.00−6.18 (br m, 202H, other Ar*H*), 4.82 (s, 102H, −SO$_3$−*CH*$_2$−CF$_3$), 4.67 (s, 50H, −O*CH*$_2$), 2.14−1.01 (br m, 250H, backbone *CH*, *CH*$_2$, CN−*CH*$_2$−S−, −S−*CH*$_2$−C$_{10}$*H*$_{20}$−CH$_3$), 0.84 (t, 3H, -C$_{11}$H$_{22}$−*CH*$_3$), 0.12 (m, 225H, Si*Me*$_3$). SEC: M_n = 107 00 g mol^{-1}; PDI = 1.17.

PTMSPS-*b*-PTfeSS 4b. PTMSPS **2b** (0.5 g, 0.04 mmol), 2,2,2-trifluoroethyl 4-vinylbenzenesulfonate (1.2 g, 4.4 mmol) and 2,2′-azobisisobutyronitrile (2.2 mg, 0.013 mmol). ^{1}H NMR (300 MHz, DMSO-d_6): δ (ppm) 7.83−7.50 (m, 100H, aromatic −*CH*═C−SO$_3$−), 7.00−6.18 (br m, 292H, other Ar*H*), 4.82 (s, 100H, −SO$_3$−*CH*$_2$−CF$_3$), 4.67 (s, 96H, −O*CH*$_2$), 2.14−1.01 (br m, 316H, backbone *CH*, *CH*$_2$, CN−*CH*$_2$−S−, −S−*CH*$_2$−C$_{10}$*H*$_{20}$−CH$_3$), 0.84 (t, 3H, −C$_{11}$H$_{22}$−*CH*$_3$), 0.12 (m, 432H, Si*Me*$_3$). SEC: M_n = 13 000 g mol^{-1}; PDI = 1.18.

PTMSPS-*b*-PTfeSS 4c. PTMSPS **2c** (0.5 g, 0.026 mmol), 2,2,2-trifluoroethyl 4-vinylbenzenesulfonate (0.7 g, 2.6 mmol) and 2,2′-azobisisobutyronitrile (1.3 mg, 0.008 mmol). ^{1}H NMR (300 MHz, DMSO-d_6): δ (ppm) 7.83−7.50 (m, 110H, aromatic −*CH*═C−SO$_3$−), 7.00−6.18 (br m, 438H, other Ar*H*), 4.82 (s, 110H, −SO$_3$−*CH*$_2$−CF$_3$), 4.67 (s, 164H, −O*CH*$_2$), 2.14−1.01 (br m, 433H, backbone *CH*, *CH*$_2$, CN−*CH*$_2$−S−, −S−*CH*$_2$−C$_{10}$*H*$_{20}$−CH$_3$), 0.84 (t, 3H, −C$_{11}$H$_{22}$−*CH*$_3$), 0.12 (m, 738H, Si*Me*$_3$). SEC: M_n = 16 900 g mol^{-1}; PDI = 1.32.

Poly(4-propargyloxy)styrene)-*block*-poly(2,2,2-trifluorethyl styrene sulfonate) (PPS-*b*-PTfeSS 5a). For deprotection of the alkyne group, PTMSPS-*b*-PTfeSS **4a** (0.9 g, 0.046 mmol) was dissolved in THF (46.2 mL) and degassed with Argon for 10 min. At −20 °C a degassed 1 M solution of tetrabutylammonium fluoride trihydrate and acetic acid (5.08 mL, 2.54 mmol) in THF was added dropwise. After 30 min at −20 °C, the temperature was raised to room temperature and the mixture was stirred for another 2 h. The resulting polymer was precipitated twice in methanol to remove the tetrabutylammonium salts. Filtration gave the deprotected polymer (0.66 g, 82%) as white powder. ^{1}H NMR (300 MHz, DMSO-d_6): δ (ppm) 7.83−7.50 (m, 102H, aromatic −*CH*═C−SO$_3$−), 7.00−6.18 (br m, 202H, other Ar*H*), 4.82 (s, 102H, −SO$_3$−*CH*$_2$−CF$_3$), 4.67 (s, 50H, −O*CH*$_2$), 3.47 (s, 25H, −C≡*CH*), 2.14−1.01 (br m, 250H, backbone *CH*, *CH*$_2$, CN−*CH*$_2$−S−, −S−*CH*$_2$−C$_{10}$*H*$_{20}$−CH$_3$), 0.84 (t, 3H, −C$_{11}$H$_{22}$−*CH*$_3$). SEC: M_n = 9800 g mol^{-1}; PDI = 1.13.

PPS-*b*-PTfeSS 5b. PTMSPS-*b*-PTfeSS **4b** (0.65 g, 0.026 mmol), 1 M solution of tetrabutylammonium fluoride trihydrate and

acetic acid (3.17 mL, 1.6 mmol). ^{1}H NMR (300 MHz, DMSO-d_6): δ (ppm) 7.83−7.50 (m, 100H, aromatic −C*H*═C−SO_3−), 7.00−6.18 (br m, 292H, other Ar*H*), 4.82 (s, 100H, −SO_3−CH_2−CF_3), 4.67 (s, 96H, −OCH_2), 3.47 (s, 48H, −C≡C*H*), 2.14−1.01 (br m, 316H, backbone *CH*, CH_2, CN−CH_2−S−, −S−CH_2−$C_{10}H_{20}$−CH_3), 0.84 (t, 3H, −$C_{11}H_{22}$−CH_3). SEC: M_n = 11 200 g mol^{-1}; PDI = 1.18.

PPS-*b*-PTfeSS 5c. PTMSPS-*b*-PTfeSS **4c** (0.65 g, 0.026 mmol), 1 M solution of tetrabutylammonium fluoride trihydrate and acetic acid (3.17 mL, 1.6 mmol). ^{1}H NMR (300 MHz, DMSO-d_6): δ (ppm) 7.83−7.50 (m, 110H, aromatic −C*H*═C−SO_3−), 7.00−6.18 (br m, 438H, other Ar*H*), 4.82 (s, 110H, −SO_3−CH_2−CF_3), 4.67 (s, 164H, −OCH_2), 3.47 (s, 82H, −C≡C*H*), 2.14−1.01 (br m, 433H, backbone *CH*, CH_2, CN−CH_2−S−, −S−CH_2−$C_{10}H_{20}$−CH_3), 0.84 (t, 3H, −$C_{11}H_{22}$−CH_3). SEC: M_n = 11 700 g mol^{-1}; PDI = 1.36.

Poly(*N*,*N*′-bis(4-methoxyphenyl)-*N*-phenyl-*N*′-4-triazolylphenyl-(1,1′-biphenyl)-4,4′-diamine)-*block*-poly(2,2,2-trifluorethyl styrene sulfonate) (PDMTPD-*b*-PTfeSS 7a). Under nitrogen, PPS-*b*-PTfeSS **5a** (0.28 g, 0.016 mmol) and DMTPD-N_3 **6** (0.29 g, 0.47 mmol) were dissolved in THF (8.7 mL) and degassed with Argon for 20 min. To start the reaction, a degassed 5 mM solution of copper(I) bromide and *N*,*N*,*N*′,*N*′,*N*-pentamethyldiethylenetriamine (0.94 mL, 4.7 μmol) in THF was added dropwise and the mixture was stirred overnight. The solvent was reduced under vacuum and the concentrated polymer was precipitated in diethyl ether. To remove the copper catalyst, the polymer was dissolved in THF and passed an Alox N column. Finally, it was again precipitated in methanol. Filtration gave 0.36 g (70%) of yellow polymer. ^{1}H NMR (300 MHz, THF-d_8): δ (ppm) 8.03−7.51 (m, 127H, Triazol-*H*, aromatic −C*H*═C−SO_3−), 7.42−6.14 (br m, 702H, other Ar*H*), 5.31 (br s, 50H, −N−CH_2-DMTPD), 4.96 (s, 102H, −SO_3−CH_2−CF_3), 4.69 (s, 50H, −OCH_2), 3.67−3.54 (m, 150H, OCH_3), 2.19−1.01 (br m, 250H, backbone *CH*, CH_2, CN−CH_2−S−, −S−CH_2−$C_{10}H_{20}$−CH_3), 0.84 (t, 3H, −$C_{11}H_{22}$−CH_3). SEC: M_n = 17 600 g mol^{-1}; PDI = 1.17.

PDMTPD-*b*-PTfeSS 7b. PPS-*b*-PTfeSS **5b** (0.5 g, 0.024 mmol), DMTPD-N_3 **6** (0.86 g, 1.42 mmol), 5 mM solution of copper(I) bromide and *N*,*N*,*N*′,*N*′,*N*-pentamethyldiethylenetriamine (2.84 mL, 0.014 mmol). ^{1}H NMR (300 MHz, THF-d_8): δ (ppm) 8.03−7.51 (m, 148H, Triazol-*H*, aromatic −C*H*═C−SO_3−), 7.42−6.14 (br m, 1252H, other Ar*H*), 5.31 (br s, 96H, −N−CH_2-DMTPD), 4.96 (s, 100H, −SO_3−CH_2−CF_3), 4.69 (s, 96H, −OCH_2), 3.67−3.54 (m, 288H, OCH_3), 2.19−1.01 (br m, 316H, backbone *CH*, CH_2, CN−CH_2−S−, −S−CH_2−$C_{10}H_{20}$−CH_3), 0.84 (t, 3H, −$C_{11}H_{22}$−CH_3). SEC: M_n = 21 600 g mol^{-1}; PDI = 1.12.

PDMTPD-*b*-PTfeSS 7c. PPS-*b*-PTfeSS **5c** (0.25 g, 8.9 μmol), DMTPD-N_3 **6** (0.54 g, 0.89 mmol), 5 mM solution of copper(I) bromide and *N*,*N*,*N*′,*N*′,*N*-pentamethyldiethylenetriamine (1.78 mL, 8.9 μmol). ^{1}H NMR (300 MHz, THF-d_8): δ (ppm) 8.03−7.51 (m, 192H, Triazol-*H*, aromatic −C*H*═C−SO_3−), 7.42−6.14 (br m, 2078H, other Ar*H*), 5.31 (br s, 164H, −N−CH_2-DMTPD), 4.96 (s, 110H, −SO_3−CH_2−CF_3), 4.69 (s, 164H, −OCH_2), 3.67−3.54 (m, 492H, OCH_3), 2.19−1.01 (br m, 433H, backbone *CH*, CH_2, CN−CH_2−S−, −S−CH_2−$C_{10}H_{20}$−CH_3), 0.84 (t, 3H, −$C_{11}H_{22}$−CH_3). SEC: M_n = 30 100 g mol^{-1}; PDI = 1.26.

Poly(*N*,*N*′-bis(4-methoxyphenyl)-*N*-phenyl-*N*′-4-triazolylphenyl-(1,1′-biphenyl)-4,4′-diamine)-*block*-poly(tetrabutylammonium styrene sulfonate) (PDMTPD-*b*-PEt$_3$NH$^+$SS 8a). PDMTPD-*b*-PTfeSS **7a** (0.2 g, 6.13 μmol) was dissolved in DMSO (5 mL). A 1 M solution of tetrabutylammonium hydroxide (1.35 mL, 1.35 mmol) in methanol was slowly added and the mixture was stirred for 24 h. The resulting polymer was precipitated in ethyl acetate and redissolved in DMF (5 mL). For exchange of the counterion, a 1 M solution of triethylamine hydrochloride (1.0 mL, 1.0 mmol) was slowly added and the polymer was again precipitated in ethyl acetate. After filtration 0.18 g (87%) of a yellow polymer were obtained. To prove the deprotection, the NMR was conducted in deuterated DMSO, which gives the best resolution for the ionic block. However, the segment comprising DMTPD aggregates in DMSO forming micellar structures. In consequence, the signals of this block are not fully resolved in the NMR analysis and they are only partially considered in the following overview. ^{1}H NMR (300 MHz, DMSO-d_6): δ (ppm) 9.10−8.86 (s, Et_3NH^+), 7.96−6.14 (br m, all Ar*H*), 3.70−3.23 (br m, OCH_3), 3.15−2.88 (q, $(CH_3-CH_2)_3$-NH^+), 2.19−1.01 (br m, backbone *CH*, CH_2, CN−CH_2−S−, −S−CH_2−$C_{10}H_{20}$−CH_3, $(CH_3-CH_2)_3$-NH^+), 0.84 (t, 3H, −$C_{11}H_{22}$−CH_3).

PDMTPD-*b*-PEt$_3$NH$^+$SS 8b. PDMTPD-*b*-PTfeSS **7b** (0.2 g, 4.0 μmol), 1 M solution of tetrabutylammonium hydroxide (1.35 mL, 1.35 mmol), 1 M solution of triethylamine hydrochloride (1.0 mL, 1.0 mmol). ^{1}H NMR (300 MHz, DMSO-d_6): δ (ppm) 9.10−8.86 (s, Et_3NH^+), 7.96−6.14 (br m, all Ar*H*), 3.70−3.23 (br m, OCH_3), 3.15−2.88 (q, $(CH_3-CH_2)_3$-NH^+), 2.19−1.01 (br m, backbone *CH*, CH_2, CN−CH_2−S−, −S−CH_2−$C_{10}H_{20}$−CH_3, $(CH_3-CH_2)_3$-NH^+), 0.84 (t, 3H, −$C_{11}H_{22}$−CH_3).

PDMTPD-*b*-PEt$_3$NH$^+$SS 8c. PDMTPD-*b*-PTfeSS **7c** (0.2 g, 2.58 μmol), 1 M solution of tetrabutylammonium hydroxide (1.35 mL, 1.35 mmol), 1 M solution of triethylamine hydrochloride (1.0 mL, 1.0 mmol). ^{1}H NMR (300 MHz, DMSO-d_6): δ (ppm) 9.10−8.86 (s, Et_3NH^+), 7.96−6.14 (br m, all Ar*H*), 3.70−3.23 (br m, OCH_3), 3.15−2.88 (q, $(CH_3-CH_2)_3$-NH^+), 2.19−1.01 (br m, backbone *CH*, CH_2, CN−CH_2−S−, −S−CH_2−$C_{10}H_{20}$−CH_3, $(CH_3-CH_2)_3$-NH^+), 0.84 (t, 3H, −$C_{11}H_{22}$−CH_3).

Conflict of Interest: The authors declare no competing financial interest.

Supporting Information Available: Synthesis of the monomers, detailed characterization of polymers including SEC and DSC, cryo-TEM of polymer solution in DMF, GISAXS analysis of as-cast and thermal annealed films, AFM images of thermal annealed samples, large area AFM images of solvent annealed samples. This material is available free of charge *via* the Internet at http://pubs.acs.org.

Acknowledgment. We thank X. Shen and B. Toga for the help with the preparation, GISAXS and TGA measurements. K. Neumann and M. Förtsch are acknowledged for the SEC and TEM measurements, respectively. Financial support from SFB 840 and the Elitenetzwerk Bayern (ENB), Macromolecular Science, (BCP synthesis and characterization) are kindly acknowledged. OPV characterization was supported by Polymer-Based Materials for Harvesting Solar Energy, an Energy Frontier Research Center funded by the U.S. Department of Energy, Office of Science, Office of Basic Energy Sciences under contract DE-SC0001087. BCP alignment and GISAXS characterization was supported by the U.S. Department of Energy, Office of Basic Energy Sciences under contract DOE-DE-FG02-45612.

REFERENCES AND NOTES

1. Orilall, M. C.; Wiesner, U. Block Copolymer Based Composition and Morphology Control in Nanostructured Hybrid Materials for Energy Conversion and Storage: Solar Cells, Batteries, and Fuel Cells. *Chem. Soc. Rev.* **2011**, *40*, 520–535.
2. Haberkorn, N.; Lechmann, M. C.; Sohn, B. H.; Char, K.; Gutmann, J. S.; Theato, P. Templated Organic and Hybrid Materials for Optoelectronic Applications. *Macromol. Rapid Commun.* **2009**, *30*, 1146–1166.
3. Förster, S.; Antonietti, M. Amphiphilic Block Copolymers in Structure-Controlled Nanomaterial Hybrids. *Adv. Mater.* **1998**, *10*, 195–217.
4. Tsarkova, L.; Sevink, G. J. A.; Krausch, G., Nanopattern Evolution in Block Copolymer Films: Experiment, Simulations and Challenges. In *Complex Macromolecular Systems I*; Müller, A. H. E., Schmidt, H.-W., Eds.; Springer: Berlin, Heidelberg: 2010; Vol. 227, pp 33−73.
5. Darling, S. B. Directing the Self-Assembly of Block Copolymers. *Prog. Polym. Sci.* **2007**, *32*, 1152–1204.
6. Hawker, C. J.; Russell, T. P. Block Copolymer Lithography: Merging "Bottom-Up" with "Top-Down" Processes. *MRS Bull.* **2005**, *30*, 952–966.
7. Thurn-Albrecht, T.; Schotter, J.; Kästle, G. A.; Emley, N.; Shibauchi, T.; Krusin-Elbaum, L.; Guarini, K.; Black, C. T.; Tuominen, M. T.; Russell, T. P. Ultrahigh-Density Nanowire Arrays Grown in Self-Assembled Diblock Copolymer Templates. *Science* **2000**, *290*, 2126–2129.
8. Morkved, T. L.; Lu, M.; Urbas, A. M.; Ehrichs, E. E.; Jaeger, H. M.; Mansky, P.; Russell, T. P. Local Control of Microdomain Orientation in Diblock Copolymer Thin Films with Electric Fields. *Science* **1996**, *273*, 931–933.
9. Rockford, L.; Liu, Y.; Mansky, P.; Russell, T. P.; Yoon, M.; Mochrie, S. G. J. Polymers on Nanoperiodic, Heterogeneous Surfaces. *Phys. Rev. Lett.* **1999**, *82*, 2602–2605.

10. Ouk Kim, S.; Solak, H. H.; Stoykovich, M. P.; Ferrier, N. J.; de Pablo, J. J.; Nealey, P. F. Epitaxial Self-Assembly of Block Copolymers on Lithographically Defined Nanopatterned Substrates. *Nature* **2003**, *424*, 411–414.
11. Chang, J.-B.; Son, J. G.; Hannon, A. F.; Alexander-Katz, A.; Ross, C. A.; Berggren, K. K. Aligned Sub-10-nm Block Copolymer Patterns Templated by Post Arrays. *ACS Nano* **2012**, *6*, 2071–2077.
12. Jung, H.; Hwang, D.; Kim, E.; Kim, B.-J.; Lee, W. B.; Poelma, J. E.; Kim, J.; Hawker, C. J.; Huh, J.; Ryu, D. Y.; *et al.* Three-Dimensional Multilayered Nanostructures with Controlled Orientation of Microdomains from Cross-Linkable Block Copolymers. *ACS Nano* **2011**, *5*, 6164–6173.
13. Hüttner, S.; Sommer, M.; Chiche, A.; Krausch, G.; Steiner, U.; Thelakkat, M. Controlled Solvent Vapour Annealing for Polymer Electronics. *Soft Matter* **2009**, *5*, 4206–4211.
14. Park, S.; Wang, J.-Y.; Kim, B.; Xu, J.; Russell, T. P. A Simple Route to Highly Oriented and Ordered Nanoporous Block Copolymer Templates. *ACS Nano* **2008**, *2*, 766–772.
15. Lee, D. H.; Park, S.; Gu, W.; Russell, T. P. Highly Ordered Nanoporous Template from Triblock Copolymer. *ACS Nano* **2011**, *5*, 1207–1214.
16. Kim, G.; Libera, M. Morphological Development in Solvent-Cast Polystyrene–Polybutadiene–Polystyrene (SBS) Triblock Copolymer Thin Films. *Macromolecules* **1998**, *31*, 2569–2577.
17. Fukunaga, K.; Elbs, H.; Magerle, R.; Krausch, G. Large-Scale Alignment of ABC Block Copolymer Microdomains *via* Solvent Vapor Treatment. *Macromolecules* **2000**, *33*, 947–953.
18. Kim, S. H.; Misner, M. J.; Xu, T.; Kimura, M.; Russell, T. P. Highly Oriented and Ordered Arrays from Block Copolymers *via* Solvent Evaporation. *Adv. Mater.* **2004**, *16*, 226–231.
19. Park, S.; Lee, D. H.; Xu, J.; Kim, B.; Hong, S. W.; Jeong, U.; Xu, T.; Russell, T. P. Macroscopic 10-Terabit–per–Square-Inch Arrays from Block Copolymers with Lateral Order. *Science* **2009**, *323*, 1030–1033.
20. Kim, E.; Ahn, H.; Park, S.; Lee, H.; Lee, M.; Lee, S.; Kim, T.; Kwak, E.-A.; Lee, J. H.; Lei, X.; *et al.* Directed Assembly of High Molecular Weight Block Copolymers: Highly Ordered Line Patterns of Perpendicularly Oriented Lamellae with Large Periods. *ACS Nano* **2013**, *7*, 1952–1960.
21. Goldberg-Oppenheimer, P.; Kabra, D.; Vignolini, S.; Hüttner, S.; Sommer, M.; Neumann, K.; Thelakkat, M.; Steiner, U. Hierarchical Orientation of Crystallinity by Block-Copolymer Patterning and Alignment in an Electric Field. *Chem. Mater.* **2013**, *25*, 1063–1070.
22. Hüttner, S.; Sommer, M.; Steiner, U.; Thelakkat, M. Organic Field Effect Transistors from Triarylamine Side-Chain Polymers. *Appl. Phys. Lett.* **2010**, *96*, No. 073503.
23. Liu, C.-L.; Lin, C.-H.; Kuo, C.-C.; Lin, S.-T.; Chen, W.-C. Conjugated Rod–Coil Block Copolymers: Synthesis, Morphology, Photophysical Properties, and Stimuli-Responsive Applications. *Prog. Polym. Sci.* **2011**, *36*, 603–637.
24. Gatsouli, K. D.; Pispas, S.; Kamitsos, E. I. Development and Optical Properties of Cadmium Sulfide and Cadmium Selenide Nanoparticles in Amphiphilic Block Copolymer Micellar-like Aggregates. *J. Phys. Chem. C* **2007**, *111*, 15201–15209.
25. Yelamanchili, R. S.; Lu, Y.; Lunkenbein, T.; Miyajima, N.; Yan, L.-T.; Ballauff, M.; Breu, J. Shaping Colloidal Rutile into Thermally Stable and Porous Mesoscopic Titania Balls. *Small* **2009**, *5*, 1326–1333.
26. Brendel, J. C.; Burchardt, H.; Thelakkat, M. Semiconductor Amphiphilic Block Copolymers for Hybrid Donor-Acceptor Nanocomposites. *J. Mater. Chem.* **2012**, *22*, 24386–24393.
27. Brendel, J. C.; Lu, Y.; Thelakkat, M. Polymer Templated Nanocrystalline Titania Network for Solid State Dye Sensitized Solar Cells. *J. Mater. Chem.* **2010**, *20*, 7255–7265.
28. Lu, Y.; Hoffmann, M.; Yelamanchili, R. S.; Terrenoire, A.; Schrinner, M.; Drechsler, M.; Möller, M. W.; Breu, J.; Ballauff, M. Well-Defined Crystalline TiO_2 Nanoparticles Generated and Immobilized on a Colloidal Nanoreactor. *Macromol. Chem. Phys.* **2009**, *210*, 377–386.
29. Moad, G.; Rizzardo, E.; Thang, S. H. Living Radical Polymerization by the RAFT Process. *Aust. J. Chem.* **2005**, *58*, 379–410.
30. Moad, G.; Chen, M.; Haussler, M.; Postma, A.; Rizzardo, E.; Thang, S. H. Functional Polymers for Optoelectronic Applications by Raft Polymerization. *Polym. Chem.* **2011**, *2*, 492–519.
31. Boyer, C.; Bulmus, V.; Davis, T. P.; Ladmiral, V.; Liu, J.; Perrier, S. b. Bioapplications of RAFT Polymerization. *Chem. Rev.* **2009**, *109*, 5402–5436.
32. Maria, S.; Susha, A. S.; Sommer, M.; Talapin, D. V.; Rogach, A. L.; Thelakkat, M. Semiconductor Block Copolymer Nanocomposites with Lamellar Morphology *via* Self-Organization. *Macromolecules* **2008**, *41*, 6081–6088.
33. Sommer, M.; Lang, A. S.; Thelakkat, M. Crystalline-Crystalline Donor-Acceptor Block Copolymers. *Angew. Chem., Int. Ed.* **2008**, *47*, 7901–7904.
34. Lang, A. S.; Thelakkat, M. Modular Synthesis of Poly(perylene bisimides) Using Click Chemistry: A Comparative Study. *Polym. Chem.* **2011**, *2*, 2213–2221.
35. Müller-Buschbaum, P. Grazing Incidence Small-Angle X-Ray Scattering: An Advanced Scattering Technique for the Investigation of Nanostructured Polymer Films. *Anal. Bioanal. Chem.* **2003**, *376*, 3–10.
36. Levine, J. R.; Cohen, J. B.; Chung, Y. W.; Georgopoulos, P. Grazing-Incidence Small-Angle X-ray Scattering: New Tool for Studying Thin Film Growth. *J. Appl. Crystallogr.* **1989**, *22*, 528–532.
37. Park, S.; Wang, J.-Y.; Kim, B.; Chen, W.; Russell, T. P. Solvent-Induced Transition from Micelles in Solution to Cylindrical Microdomains in Diblock Copolymer Thin Films. *Macromolecules* **2007**, *40*, 9059–9063.
38. Lechmann, M. C.; Kessler, D.; Gutmann, J. S. Functional Templates for Hybrid Materials with Orthogonal Functionality. *Langmuir* **2009**, *25*, 10202–10208.
39. Javier, A. E.; Patel, S. N.; Hallinan, D. T.; Srinivasan, V.; Balsara, N. P. Simultaneous Electronic and Ionic Conduction in a Block Copolymer: Application in Lithium Battery Electrodes. *Angew. Chem., Int. Ed.* **2011**, *50*, 9848–9851.